Online Heat Pattern Control of Ferro-Coke Furnace Based on Data Assimilation

HASHIMOTO Yoshinari[*1] ANYASHIKI Takashi[*2] FUJIMOTO Hidekazu[*3] TSUDA Kazuro[*4]

Abstract:

In steel works, direct observation of internal conditions of high temperature processes is difficult. Therefore, automation of such processes based on process visualization is an urgent issue. The authors developed a technique that controls the heat pattern of a shaft furnace by visualizing internal conditions by means of a particle filter, which combines sensor information and a transient two-dimensional model calculation. As a result of the validation test at the ferro-coke pilot plant, control accuracy of 10°C was achieved. Furthermore, the operational condition was adjusted based on the correlation between the estimated heat pattern and the product strength. In consequence, the product strength improved by 0.5 points (Drum Index 150/15 mm, DI^{150}_{15}).

1. Introduction

The steel industry employs a large number of reaction processes using shaft furnaces, beginning with the blast furnace. Operation of the reaction processes is still performed manually by operators since real-time measurement of the internal state of those processes is normally difficult. The manual operation depends on the operator's experience and intuition, and automation of these "black-box" processes by visualization of the internal state is an urgent issue. This paper introduces a heat pattern control logic based on visualization of the internal state of a ferro-coke furnace by the integration of a transient model and sensor information, that is, data assimilation.

Ferro-coke is a type of high-reactive formed carbon briquette that is produced by blending coal and fine iron ores at a ratio of 7 : 3. Because the coke gasification reaction begins from a lower temperature compared with conventional coke in a blast furnace, the ferro-coke is expected to have the effect of decreasing the reducing agent ratio (RAR) by reducing the temperature of the thermal reserve zone [1, 2]. The ferro-coke furnace used to produce ferro-coke is a continuous counterflow heat exchange process in which solid raw materials are charged from the furnace top and the product is discharged from the furnace bottom. The residence time of the solids in the furnace is approximately 10 hours. The heat pattern is subject to constraints on the temperature rising rate, coking time, and cooling. For example, a faster temperature rising rate enhances the fluidity of the coal particles, resulting in higher product strength, and the residence time in the high-temperature region (*i.e.*, the coking region) must be within the proper range in order to ensure both product strength and reactivity [2, 3].

Although the control of the heat pattern of the entire furnace is necessary, the positions where temperature sensors can be installed are limited. Unknown parameters that are difficult to measure online, such as

† Originally published in *JFE GIHO* No. 45 (Feb. 2020), p. 32−38

*1 Dr. Inf.,
Senior Researcher Deputy Manager,
Cyber-Physical System Research & Development Dept.,
Steel Res. Lab.,
JFE Steel

*2 Senior Researcher General Manager,
Ironmaking Research Dept.,
Steel Res. Lab.,
JFE Steel

*3 Dr. Eng.,
Senior Researcher Deputy General Manager,
Ironmaking Research Dept.,
Steel Res. Lab.,
JFE Steel

*4 Staff General Manager,
Data Science Project Dept.,
JFE Steel

heat loss from the furnace wall and the specific heat of the solid, also exist in a ferro-coke furnace. The fluctuations of these parameters cause estimation errors in calculations by conventional transient models using fixed parameters. Therefore, in this research, the internal state in the furnace was visualized by the combination of transient model calculations and partial sensor information, and an algorithm that controls the heat pattern to a required condition was constructed [4].

The particle filter [5] was adopted as a technique for the data assimilation which integrates sensor information and model calculations. Multiple nonlinear transient models that involve various unknown parameter groups are calculated online in parallel and the unknown parameters are estimated online by successively updating the weight of each model using the sensor data. This approach enables online estimation corresponding to temporal changes in the plant with a clear physical interpretation.

This report describes the visualization of the internal state of the ferro-coke furnace by the particle filter technique, the results of validation of heat pattern control in a pilot plant, and expansion of this technique to the improvement of ferro-coke quality.

2. Visualization of Furnace Internal State by Data Assimilation

The ferro-coke furnace has a shaft structure, as illustrated in **Fig. 1**, in which gas injection ports (tuyeres) are installed symmetrically on opposing sides of the shaft. These tuyeres comprise three types, which are termed low-temperature tuyere, hot tuyere (high-temperature tuyere), and cooling tuyere. The low-temperature tuyere has the function of adjusting the temperature rising rate in the upper part of the furnace, and the hot tuyere is used to secure the requisite holding time in the high-temperature region. A product discharge device and cooling tuyere are installed in the lower part of the furnace. The raw materials charged from the furnace top undergo heat exchange with high-temperature gas and are carbonized during descending through the furnace. Finally, the product is discharged from the furnace after heat exchange with the cooling gas.

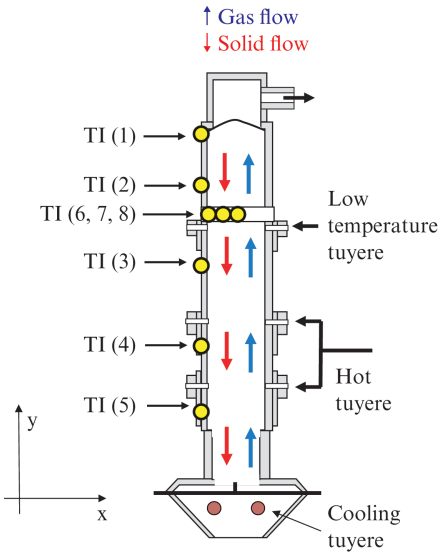

Fig. 1 Structure of ferro-coke furnace

To estimate the temperature distribution in the ferro-coke furnace heat, a two-dimensional (2D) transient model that considers the reaction, flow, and heat transfer in the furnace was developed, where the two dimensions are the x and y directions shown in Fig. 1. The gas flow follows Ergun's equation [6], and the solid flow was simplified as a simple vertical descent. The heat transfer phenomena comprise heat exchange between the gas and solid, heat exchange between the gas and atmosphere surrounding the furnace (via the furnace wall), and the reaction heat. Gasification of the volatile fraction of the coal and the gas reduction reaction of iron oxide (iron ore) in the furnace were also considered. The equations for obtaining the gas temperature and solid temperature are as shown in Eqs. (1) and (2).

$$\frac{\partial\left(\rho_g C_{p,g} T_g\right)}{\partial t}+\frac{\partial\left(C_{p,g} u_g T_g\right)}{\partial x}+\frac{\partial\left(C_{p,g} v_g T_g\right)}{\partial y}= S\alpha\left(T_s-T_g\right)+R\Delta H_R\eta_g+h\left(T_o-T_g\right) \quad \ldots\ldots (1)$$

$$\frac{\partial\left(\rho_s C_{p,s} T_s\right)}{\partial t}+\frac{\partial\left(\rho_s C_{p,s} v_s T_s\right)}{\partial y}=S\alpha\left(T_g-T_s\right)+R\Delta H_R\eta_s \quad \ldots\ldots (2)$$

where the subscripts s, g, and o mean solid, gas, and outside atmosphere surrounding the furnace, respec-

Table 1 Variables in transient 2D model

Symbol	Notes	Unit
C_p	Specific heat	J/kg/K
h	Heat-loss coefficient	J/m^3/s
R	Reaction rate	kg/m^3/s
S	Specific surface area	m^2/m^3-bed
T	Temperature	K
u_g	Mass velocity of gas (horizontal)	kg/m^2/s
v_g	Mass velocity of gas (vertical)	kg/m^2/s
v_s	Velocity of solid (vertical)	m/s
α	Heat exchange coefficient	J/m^2/s
ΔH_R	Reaction heat	J/kg
η	Reaction heat distribution ratio	–
ρ	Density	kg/m^3

tively. The variables in the 2D transient model are listed in **Table 1**.

The differential equations for the furnace phenomena in Eqs. (1) and (2) were discretized by the finite volume method and full-implicit method. The time step was 10 minutes. In the following, these discretized equations are expressed in the form of the state-space model shown in Eqs. (3) and (4), *i.e.*, update rule of temperature distribution in time-step units.

$$\mathbf{T}(t+1)=f\left(\mathbf{T}(t),\mathbf{u}(t),\mathbf{A}(t)\right) \quad \cdots\cdots (3)$$

$$\mathbf{y}(t)=\mathbf{C}\mathbf{T}(t) \quad \cdots\cdots (4)$$

where $\mathbf{T}(t)$ is the temperature distribution of the solid and gas at time step t, and the number of elements is two times the computational mesh number of the 2D transient model. $\mathbf{u}(t)$ represents the inflow gas volume from each tuyere and its temperature, which are the model inputs, and $\mathbf{A}(t)$ is the unknown parameters. In this research, the two parameters, the specific heat of solid $C_{p,s}$ and coefficient of heat loss from furnace wall to the atmosphere h, were set as the unknown parameters. $\mathbf{y}(t)$ is the temperature at the sensor (thermocouple) position, and the matrix $\mathbf{C}$ is the observation matrix, which extracts elements corresponding to the sensor position from the temperature distribution $\mathbf{T}(t)$.

The algorithm of the particle filter consists of the following five steps. In comparison with conventional fixed parameters, highly accurate estimation is possible by data assimilation of partial sensor information and model calculations and successive online identification of parameters. **Figure 2** shows an overview of the algorithm.

Step 1: First, N physical models assuming different unknown parameters are prepared. In this research, N = 25. The initial weight w of each model is given by Eq. (5)

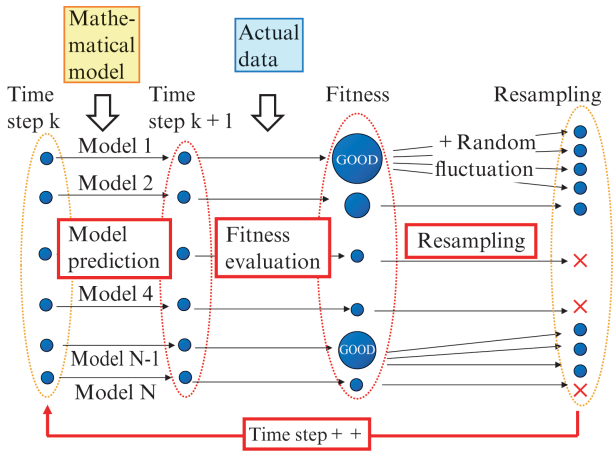

Fig. 2 Algorithm of particle filter

$$w_i=1/N \quad \cdots\cdots (5)$$

where the subscript i means the index of the respective models.

Step 2: The temperature distributions of each model are calculated in parallel by using the state-space model.

$$\mathbf{T}_i(t+1)=f\left(\mathbf{T}_i(t),\mathbf{u}(t),\mathbf{A}_i(t)\right) \quad \cdots\cdots (6)$$

$$\mathbf{y}_i(t)=\mathbf{C}\mathbf{T}_i(t) \quad \cdots\cdots (7)$$

Step 3: The likelihood θ_i (t), corresponding to the degree of coincidence with the actual value $\mathbf{y}_{\mathrm{act}}$ (t) of the temperature measured by the thermocouple, is calculated.

$$\theta_i(t)=\exp\left(-\frac{\left|\mathbf{y}_i(t)-\mathbf{y}_{\mathrm{act}}(t)\right|^2}{\sigma^2}\right) \quad \cdots\cdots (8)$$

where σ^2 is the estimated square error of all models.

$$\sigma^2=\sum_{i=1}^{N}\frac{\left|\mathbf{y}_i(t)-\mathbf{y}_{\mathrm{act}}(t)\right|^2}{N} \quad \cdots\cdots (9)$$

Step 4: The weight of each model is updated based on Bayes' theorem. The weights of the models are normalized so that the total weight of all models is unity.

$$w_i(t)\propto w_i(t-1)\theta_i(t) \quad \cdots\cdots (10)$$

$$\sum_i w_i(t)=1 \quad \cdots\cdots (11)$$

The estimations of the temperature distribution and the unknown parameters, which are the outputs of data assimilation, are calculated as the weighted average of all models.

$$\mathbf{T}_{\mathrm{a}}(t)=\sum_i w_i(t)\cdot\mathbf{T}_i(t) \quad \cdots\cdots (12)$$

$$\mathbf{A}_{\mathrm{a}}(t)=\sum_i w_i(t)\cdot\mathbf{A}_i(t) \quad \cdots\cdots (13)$$

Step 5: Copies of the models are generated with a probability proportional to the weight of each model, and the unknown parameters for each model are disturbed slightly by adding a random fluctuation to avoid multiple models with completely identical parameters. Following this step, the time step is updated, and the calculation process returns to Step 2.

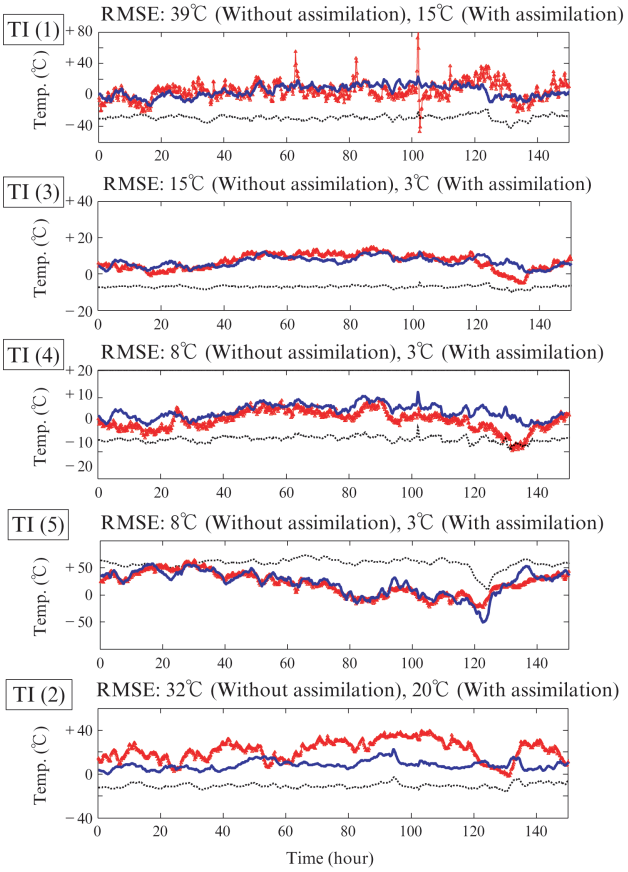

Fig. 3 Estimation result of surface temperature

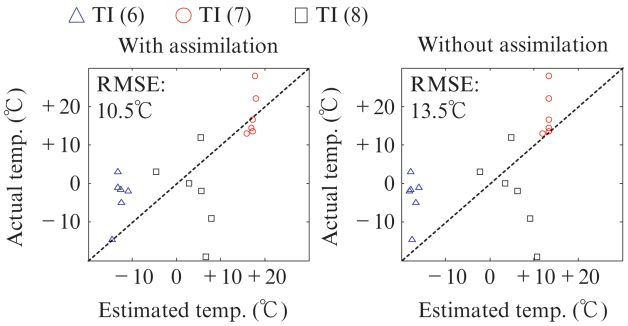

Fig. 4 Estimation result of internal temperature

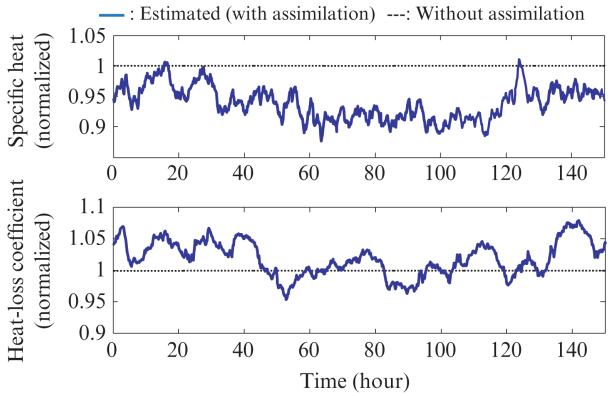

Fig. 5 Estimation result of unknown paramters

3. Validation result at Pilot Plant

The heat pattern visualization system using a particle filter described in the previous chapter was implemented in the operation room of a pilot plant. Among the five furnace-wall thermocouples (TI(1) to TI(5)) shown in Fig. 1, the four thermocouples other than TI(2) were used in assimilation with the model. TI(2) was used for validation, and it was not used for assimilation.

First, the results of validation by the thermocouples for assimilation are described. In **Fig. 3**, the bold red lines show the actual values, the solid blue lines show the estimated values with assimilation and the broken black lines show the estimated results without assimilation. (A calculation of one model in which the unknown parameters were fixed was performed offline.) The vertical axes show the deviation from the target value. As an index of estimation error, the root mean square error (RMSE) is also shown in the figure. In the upper four rows in Fig. 3, the estimation error with data assimilation was reduced by an average of 50% or more in comparison with the case without assimilation.

Next, the results obtained with the thermocouple for validation are described. In the results of the validation thermocouple shown in the bottom row of Fig. 3, the estimation error was also reduced by 40% by data assimilation. **Figure 4** shows the estimation results of the internal temperature (TI(6) to TI(8)) in Fig. 1. Here, the internal temperature is obtained by using a horizontal probe which is inserted into the furnace intermittently. The estimation error of the internal temperature was also reduced by 30%. Although parameter estimation is susceptible to the problem of over-fitting, this problem did not occur since the estimation error of the validation thermocouple also decreased.

Figure 5 shows the estimation results for the specific heat of solid and the heat-loss coefficient, which were the unknown parameters. The contact between the furnace wall and the burden or a biased flow of gas in the furnace might cause fluctuations in the heat-loss coefficient. The change in the amount of coking heat due to changes in the coal brand is a possible explanation for the fluctuations of the specific heat.

The validation results described above confirmed that the estimation accuracy of the temperature distribution was improved by the particle filter logic.

4. Establishment of Heat Pattern Control Logic

Next, a control algorithm for maintaining the heat pattern in a required condition was developed based on

the estimation by data assimilation. The control algorithm comprises the following three steps. First, the future heat pattern is predicted assuming the current input variable is maintained; next, the step response when the manipulated variable is changed is calculated; and finally, the optimum control action of the manipulated variable is determined. The control period was set at 10 minutes. The following describes the control algorithm, in which the manipulated variables are the flow rates of the hot tuyere and the cooling tuyere, and the controlled variables are the gas temperature at the furnace top, the discharge temperature of the product at the furnace bottom, and the internal temperature.

First, the future controlled variables are estimated based on Eqs. (14) and (15), assuming that the present input variables are kept constant in the future.

$$\mathbf{T}(t+k+1) = f\left(\mathbf{T}(t+k), \mathbf{u}(t), \mathbf{A}(t)\right) \quad \cdots\cdots (14)$$

$$\mathbf{z}(t+k) = \mathbf{H}\mathbf{T}(t+k) \quad \cdots\cdots (15)$$

where t is the present time step and k takes the values from 0 to 48 in order to carry out prediction up to 8 hours in the future. $\mathbf{z}(t)$ represents the controlled variables, and $\mathbf{H}$ is a matrix that extracts the controlled variable from the estimated temperature distribution. The heat pattern and parameters estimated by Eqs. (12) and (13) were used as the initial conditions of the prediction.

$$\mathbf{T}(t) = \mathbf{T}_a(t) \quad \cdots\cdots (16)$$

$$\mathbf{A}(t) = \mathbf{A}_a(t) \quad \cdots\cdots (17)$$

The trend of the controlled variables (top gas temperature, discharge temperature, internal temperature) calculated in this manner is denoted as the free response $\mathbf{z}_f(t) = \left[z_f^1(t), z_f^2(t), z_f^3(t)\right]^T$.

Next, the step responses of the controlled variables when the manipulated variables are changed are calculated. The step responses depend greatly on the operational condition and unknown parameters. To deal with this nonlinearity, the step responses are updated in each control period by the following procedure.

The change of the controlled variables is predicted in case each manipulated variable is changed only by a unit amount. Let the response of the controlled variable when the flow rate of the hot tuyere is changed by ΔF be $\mathbf{z}_1(t)$ and the response when the flow rate of the cooling tuyere be changed by ΔF be $\mathbf{z}_2(t)$. The step response of the controlled variable j (= 1, 2, 3) to the manipulated variable i (= 1, 2) is calculated by the following Eq. (18).

$$S_i^j(t+k|t) = \left(z_i^j(t+k) - z_f^j(t+k)\right) / \Delta F \quad \cdots\cdots (18)$$

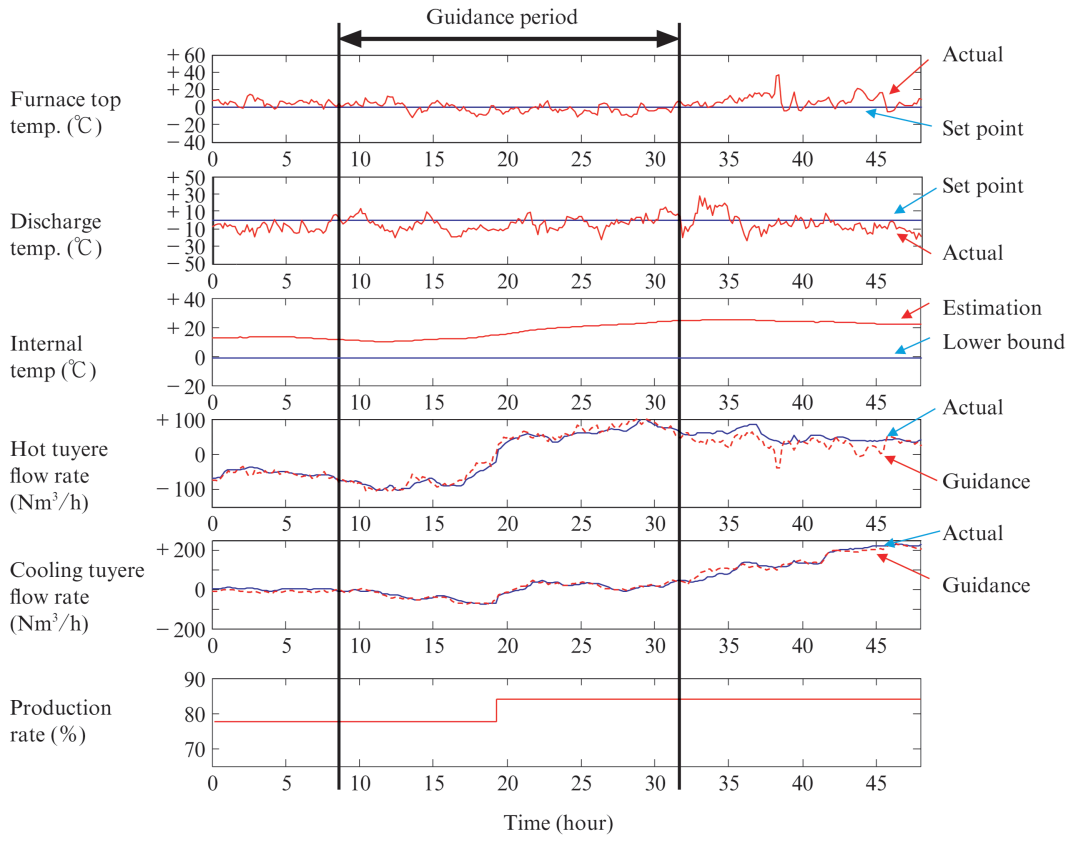

Fig. 6 Experimental result of heat pattern control at pilot plant

Finally, the optimal control action for the manipulated variables is obtained. Using quadratic programming, the amount of actions ΔF_1 and ΔF_2 of the manipulated variables is obtained to minimize the cost function J shown in Eq. (19) under the constraints in Eq. (20).

$$J = \sum_{k=1}^{48}\sum_{j=1}^{2}\left(z_{\mathrm{p}}^{j}(t+k) - z_{\mathrm{r}}^{j}\right)^2 + \sum_{i=1}^{2} b_i \left(\Delta F_i\right)^2 \quad \cdots\cdots \quad (19)$$

$$z_{\mathrm{p}}^{3}(t+k) \geq z_{\mathrm{L}}^{3} \quad \cdots\cdots \quad (20)$$

where $\mathbf{z}_{\mathrm{r}}$ is the set point of the controlled variable and $\mathbf{z}_{\mathrm{L}}$ is the lower limit of the controlled variable. $\mathbf{z}_{\mathrm{p}}(t) = \left[z_{\mathrm{p}}^{1}(t), z_{\mathrm{p}}^{2}(t), z_{\mathrm{p}}^{3}(t)\right]^T$ are the predicted values of the controlled variable when the manipulated variable is changed, and they were approximated by a linear combination of the free response and the step responses, as shown in Eq. (21).

$$z_{\mathrm{p}}^{j}(t+k) = z_{\mathrm{f}}^{j}(t+k) + \sum_{i=1}^{2} S_i^j(t+k|t)\Delta F_i \quad (j=1,2,3)$$

$$\cdots\cdots \quad (21)$$

The control algorithm described above was implemented in a pilot plant and an operation test in the guidance form was conducted. The results are shown in **Fig. 6**. The top three rows show the controlled variables, the 4th and 5th rows show the manipulated variables and the bottom row shows the production rate. For the manipulated variables, the guidance value and actual value are plotted. The manipulated variables were changed following the output of the control system during the guidance period from 8 h to 32 h in this figure.

During the guidance period, the production rate increased at 19 h. Accompanying this change, a decrease in the furnace top temperature and an increase in the discharge temperature was predicted, and the control action to increase the hot tuyere flow rate and cooling tuyere flow rate was output. As a result of manipulation of the tuyere flow rates in accordance with this guidance, it was possible to keep the furnace top temperature and discharged temperature in the range of the set point ±10°C, while continuing to observe the lower limit of the internal temperature.

5. Correlation of Estimated Heat Pattern and Product Quality

Heat pattern control to ensure the product quality is one conceivable method for utilizing heat pattern visualization by this logic. Therefore, the correlation between the visualized heat pattern and product strength was analyzed to identify the factors that determine product strength.

As shown in **Fig. 7**, the furnace was divided into four zones in the vertical direction, and the calculated temperature history of the burden material in the process of descending through the furnace was calculated for each zone. Calculation of the temporal pattern in this manner made it possible to compare data with different burden descent rates (production rates) by the same criterion. In addition, the characteristic values of the heat pattern in each of the four zones were also calculated, and the correlation between the averaged characteristic value of the four zones and product strength was investigated.

As a result, it was found that there is a negative correlation between product strength and holding time in the high-temperature zone where the temperature is higher than 75%, as shown in **Fig. 8**. The red line in this figure is the regression line by the least square method. The strength of normal chamber-oven type coke is enhanced by longer coking times because the coke microstructure approaches the graphite structure. However, in the case of ferro-coke, excessive coking could lead to a decrease in the strength because the coke surrounding the iron ore is partially consumed in the reduction of the ore, resulting in a porous structure.

Based on the results of this correlation analysis, the temperature distribution was simulated for the case of

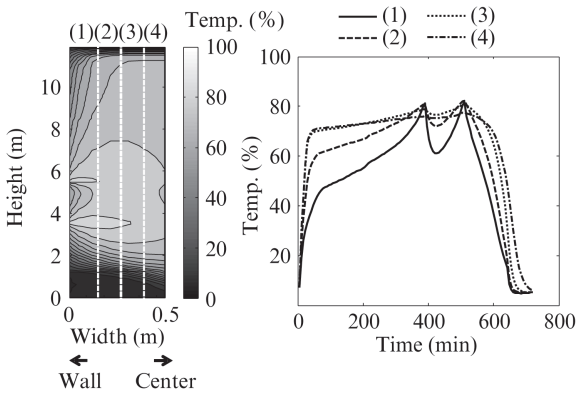

Fig. 7 Temperature history of ferro-coke

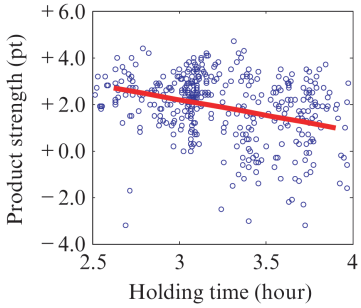

Fig. 8 Correlation between holding time in high temperature zone and ferro-coke strength

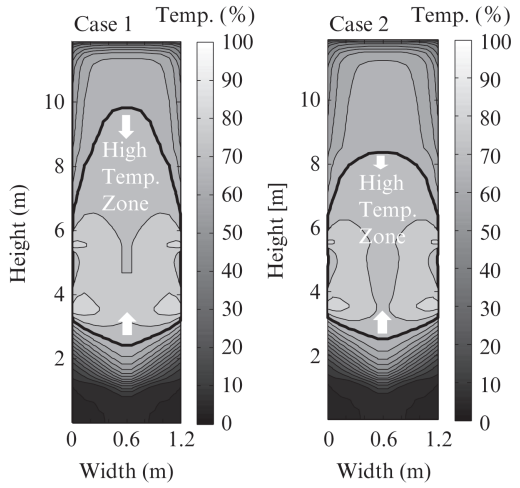

Fig. 9 Steady-state simulation result of temperature distribution

gas blowing from the low-temperature tuyere, which had not been actively used in conventional operation. **Figure 9** shows the calculated temperature distribution in the steady state under the simulation conditions in **Table 2**. Since it is possible to shorten the ferro-coke holding time in the high-temperature region by increasing the flow rate of the low-temperature tuyere and decreasing that of the hot tuyere, it is thought that improved product strength can be expected.

Based on this simulation, the operation of the pilot plant was carried out under the conditions of Case 2 in Table 2, and as a result, product strength increased by 0.5 points (Drum Index 150/15 mm, $DI^{150}15$) [4].

This result shows that manipulation of the feature value of the estimated heat pattern contributes to quality improvement, and it supports the effectiveness of the proposed approach.

6. Conclusion

In this research, the internal state in a ferro-coke furnace was visualized by combining a two-dimensional transient model based on particle filter logic and partial sensor information, and a control algorithm to maintain the heat pattern in the desired state was developed. Control accuracy of 10˚C was achieved at a ferro-coke pilot plant. In addition, the operational conditions of the pilot plant were optimized based on an analysis of the correlation between the product strength and the estimated heat pattern, and the product strength (Drum Index 150/15, $DI^{150}15$) was improved by 0.5 points.

Table 2 Operational condition of ferro-coke furnace

	Case1 (base)	Case2
Low temp. tuyere	50 Nm^3/h	300 Nm^3/h
Hot tuyere	2 050 Nm^3/h	1 920 Nm^3/h
Cooling tuyere	2 400 Nm^3/h	2 400 Nm^3/h
Holding time in high temperature zone	3.2 h	2.5 h

This research was carried out as part of the project "Technological Development of Innovative Ironmaking Process to Enhance Resource Flexibility" of Japan's New Energy and Industrial Technology Development Organization (NEDO). The authors wish to thank all those concerned.

References

1) Nomura, S.; Kitaguchi, S.; Yamaguchi, K.; Naito, M. The Characteristics of Catalyst-coated Highly Reactive Coke. ISIJ Int., 2007, vol.47, p. 245–253.
2) Yamamoto, T.; Sato, T.; Fujimoto, H.; Anyashiki, T.; Fukada, K.; Sato, M.; Takeda, K.; Ariyama, T. Reaction Behavior of Ferro Coke and Its Evaluation in Blast Furnace. Tetsu-to-Hagane, 2011, vol. 97, p. 501–509.
3) Ando, M.; Iwai, Y.; Fujimoto, H.; Sato, T.; Hashimoto, Y.; Anyashiki, T.; Sato, M. Development of Numerical Thermo-fluid Simulator of Ferro Coke Shaft Furnace. Tetsu-to-Hagane, 2018, vol. 104, p. 543–550.
4) Hashimoto, Y.; Tsuda, K.; Anyashiki, T.; Fujimoto, H. Online heat pattern control of a shaft furnace based on a real-time visualization by particle filter. ISIJ Int., 2017, vol. 57, p. 131–138.
5) Rawlings, J.B.; Bakshi, B.R. Particle filtering and moving horizon estimation. Computers and Chemical Engineering, 2006, vol. 30, p. 1529–1541.
6) Ergun, S. Fluid flow through packed columns. Chem. Eng. Prog., 1952, vol. 48, p. 89–94.